Modeling Lightweight High-Temperature Expandable Radiator Structures for Space-Based Nuclear Power Systems and Small Satellites in Low Earth Orbit (LEO)

M. Crews
Department of Physics, University of Nebraska Omaha, Omaha, Nebraska 68182

K. Kwok and Bojan Bijelic
Department of Mechanical and Aerospace Engineering, University of Central Florida, Orlando, FL, 32816, USA

(Dated: May 12, 2024)

Advancements in technology and engineering have led to the development of cutting-edge radiator materials and designs, enabling spacecraft to operate at higher temperatures. This is crucial for nuclear-powered systems and small satellites, both of which demand innovative solutions. The intense heat generated by space-based nuclear power systems and hypersonic vehicles poses a significant challenge to spacecraft structural integrity. To address this, we propose a method that rapidly approximates thermal parameters during the initial modeling phase, allowing us to identify the most promising radiator designs efficiently. While constructing a model involves various considerations, we offer an approach using solid-state and thermodynamic calculations, only taking the maximum parameters into consideration. Our model overview outlines the thermal design process, showcasing our methods for assessing radiator design viability.

I. NOMENCLATURE:

A_{cell} = Surface area of solar cells
$A_{\oplus}$ = Cross sectional area
A_{eff} = Effective area
ALB = Albedo factor
ALT = Altitude
A_{p} = Surface area of solar panel
A_{tot} = Total surface area
$F_{1\to2}$ = View factor
Q_{in} = Heat supplied
Q_{out} = Heat rejected
q_{alb} = Heat supplied via albedo radiation
q_{IR} = Heat supplied via infrared Earth radiation
q_{gen} = Heat supplied via internal generation
q_{rad} = Heat rejected via radiator
$q_{\odot}$ = Heat supplied via solar radiation
$q_{\text{alb},f}$ = Heat flux supplied via albedo radiation
$q_{\text{IR},f}$ = Heat flux supplied via infrared Earth radiation
$q_{\odot,f}$ = Heat flux supplied via solar radiation
R_{E} = Radius of Earth
r_{cir} = Radius of circle
S = Solar constant
T = Temperature
T_{eff} = Effective temperature
α_{c} = Absorptivity of solar cell
$\alpha_{\text{c,eff}}$ = Effective absorptivity of solar cell
α_{eff} = Effective absorptivity
$\alpha_{\text{pan,eff}}$ = Effective absorptivity of solar panel
$\varepsilon_{\text{c,eff}}$ = Effective emissivity of solar cell
ε_{eff} = Effective emissivity
$\varepsilon_{\text{pan,eff}}$ = Effective emissivity of solar panel
η = Efficiency
σ = Stefan-Boltzmann constant
ϕ = Incident angle

II. INTRODUCTION

The thermal design process in this review is founded on three key concepts outlined by the United States Space Force (USSF) in the Small Satellite Thermal Modeling Guide [1]. This process comprises thermal modeling, thermal analysis, and thermal control. While these terms are sometimes used interchangeably, it's crucial to differentiate them. In the context of this work, thermal modeling involves mathematically describing the spacecraft's thermal characteristics. Once we have the outputs, we move into the thermal analysis phase, where we analyze the established parameters. Thermal control is the selective process in which the best candidate is chosen for further testing. Although these concepts are distinct, they work together, influencing one another as outlined in Figure 1.

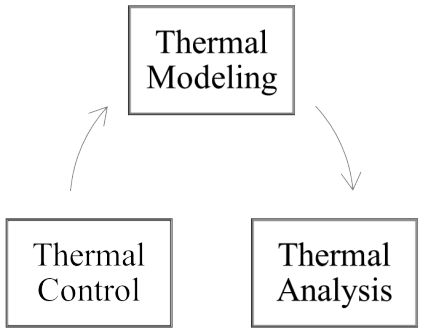

FIG. 1. Cyclical process of thermal design

The study of thermodynamics in Low Earth Orbit (LEO) spacecraft has advanced significantly in current literature. Mapping and calculating heat paths, both internal and external, are typically straightforward. However, as

parameters require more precision, a flexible mathematical model becomes essential. This work aims to develop a model for rapid analysis of radiator designs through three distinct modeling phases:

i. Thermal Environment

ii. Radiator Material

iii. Experiment

Each phase utilizes MATLAB software for mathematical analysis, providing a comprehensive guide in the "LIVE EDITOR" tab. This modeling process is iterative, focusing on a steady-state model initially. Future work will expand the model to include time-dependent variables, non-terrestrial orbits, interstellar travel simulations, and scaling up for spacecraft with nuclear power systems. Additionally, addressing the energy output challenges from nuclear spacecraft will be explored.

III. EFFICIENT THERMAL HAND CALCULATIONS MODEL FOR SATELLITES IN LEO

A. Overview

Heat is the change in internal energy of a system when no work is done on or by the system [2]. An essential aspect of the first law of thermodynamics is the conservation of energy, with heat being a form of energy that can be transferred into a system, leading to a change in its internal energy minus any work involved in the process. Spacecraft are designed with specific temperature ranges to avoid overheating or excessive cooling, crucial for meeting operational and survival requirements [3]. We initially consider a system where our spacecraft is defined as a stationary, heterogeneous, and anisotropic solid. In a general scenario, the heat exchange is represented by the equation $Q_{\text{in}} = Q_{\text{out}}$. Figure 2 illustrates the simplified thermal environment for a small satellite in Earth's orbit.

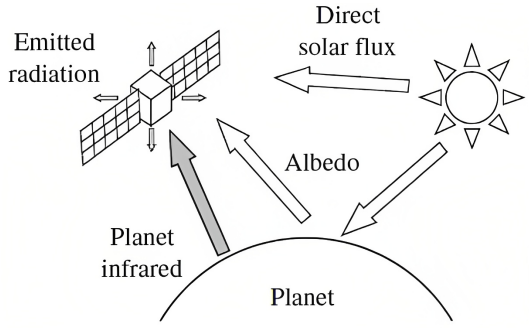

FIG. 2. Cyclical process of thermal design

Thus, based on these sources of radiation, the thermal balance equation can be expressed as,

$$q_{\oplus} + q_{\text{alb}} + q_{\text{IR}} = Q_{\text{rad}}. \tag{1}$$

Our model is constructed using the equations specified in the USSF: Small Satellite Thermal Modeling Guide [1]. This guide compares calculations to the literature values of the Innovative Solutions in Space's (ISISPACE) 3U SmallSat. By incorporating these equations into our model, users can easily adjust variables to suit any particular satellite. The primary objective is to employ maximum parameters for rigorous threshold testing.

B. Thermal Environment Modeling Process

To demonstrate and validate our concept, we can efficiently confirm the handbook's calculations of ISISPACE 3U SmallSat values with greater efficiency, while maintaining low cost. Initially, we document the constants and provided parameters, which are presented in the table below. The dimensions of a 3U SmallSat are 30 cm×10 cm×10 cm, with a total surface area of approximately 1400 cm^2. Initially, we convert the surface area from that of a rectangular prism to that of a sphere. This conversion will enable us to determine the cross-sectional area and the view factor subsequently. Equations (2) and (3) outline the calculation for the cross-sectional area.

$$A_{\text{tot}} = 4\pi r_{\text{cir}}^2 \rightarrow r_{\text{cir}} = \sqrt{\frac{A_{\text{tot}}}{4\pi}} \tag{2}$$

$$A_{\oplus} = \pi r_{\text{cir}}^2 \tag{3}$$

This model consists of spatially averaged absorptivity and emissivity values based on the chosen spacecraft's solar panel. For the purpose of this work, we will separate the panel and cells into two categories, both together will be expressed as "Effective". Values are subject to change based on the experimental data and can be swapped out with ease. The modeled area for the solar panel and cells are obtained antecedently. The effective absorptivity and emissivity for the solar panel are determined experimentally beforehand. While the solar cell's effective emissivity is provided, the effective absorptivity needs to be calculated. An absorptivity value of 0.910 is recorded, hence, the effective solar cell absorptivity can be calculated by using Equation (4).

$$\alpha_{\text{c,eff}} = \alpha_{\text{c}}(1 - \eta) \tag{4}$$

Now to determine the effective area, absorptivity, and emissivity, the following three equations are utilized:

$$A_{\text{eff}} = \sum_{j=1}^{n} A_j \tag{5}$$

$$\alpha_{\text{eff}} = \sum_{j=1}^{n} \left(\frac{A_j}{A_{\text{tot}}} \right) \alpha_j \tag{6}$$

$$\varepsilon_{\text{eff}} = \sum_{j=1}^{n} \left(\frac{A_j}{A_{\text{tot}}} \right) \varepsilon_j \tag{7}$$

Here, the subscript j is used to denote the area, absorptivity, or the emissivity of an individual component. Another crucial variable to consider is the radiation view factor. Having transformed the spacecraft's surface area into a sphere, we can apply Equation (8) to calculate this factor.

$$F_{1\to 2} = \frac{1}{2}\left(1 - \sqrt{1 - \frac{1}{h^2}}\right), \quad h = \frac{R_{\text{E}} + \text{ALT}}{R_{\text{E}}} \tag{8}$$

All variables have now been established and we can proceed with heat calculations. Each heat source represents its own equation, where both the flux and transfer are calculated. These equations can be seen below. The absorbed solar radiation will utilize the cross sectional area while the absorbed albedo and IR radiation will use the total area of the spacecraft.

$$q_{\odot,f} = \alpha_{\text{eff}} S \cos\theta \tag{9}$$

$$q_{\text{alb},f} = \alpha_{\text{eff}} S F_{1\to 2} \text{ALB} \tag{10}$$

$$q_{\text{IR},f} = \sigma \varepsilon_{\text{eff}} F_{1\to 2} T_{\text{eff}}^4 \tag{11}$$

$$q_{\odot} = \alpha_{\text{eff}} A_{\oplus} S \cos\theta \tag{12}$$

$$q_{\text{alb}} = \alpha_{\text{eff}} A_{\text{tot}} S F_{1\to 2} \text{ALB} \tag{13}$$

$$q_{\text{IR}} = \sigma \varepsilon_{\text{eff}} A_{\text{tot}} F_{1\to 2} T_{\text{eff}}^4 \tag{14}$$

By utilizing each heat value, we can now determine the steady-state temperature of the satellite. The total heat input can be calculated using Equation (15) provided below.

$$q_{\text{in}} = \sum_{i=1}^{L} q_{\odot,i} + \sum_{j=1}^{M} q_{\text{alb},j} + \sum_{k=1}^{N} q_{\text{IR},k} = Q_{\text{out}} \tag{15}$$

Here, the subscripts i, j, and k correspond to the individual surfaces, where L, M, and M are the maximum number of surfaces. Since $Q_{\text{out}} = Q_{\text{rad}}$, we can employ Equation (16) to compute the operating temperature, leading to Equation (17).

$$Q_{\text{rad}} = \sum_{i=1}^{n} A_i \varepsilon_i \sigma T_i^4 \tag{16}$$

$$T = \left(\frac{Q_{\text{rad}}}{A_{\text{tot}} \varepsilon_{\text{eff}} \sigma} \right) \tag{17}$$

The subscript i refers to i^{th} surface while the superscript n denotes the maximum number of radiative surfaces. Now that the validity of the model has been confirmed, the maximized results can be seen in the proceeding section. Below is a graph confirming the ISISPACE 3U SmallSat data.

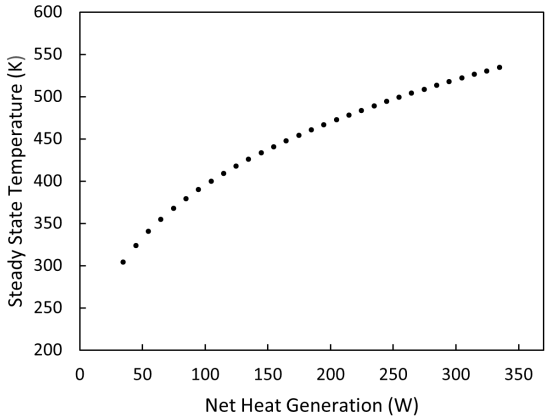

FIG. 3. Example graph of temperature vs net heat generation from MATLAB data

C. Results

After running all sections, the model outputs a data set to be represented graphically. The type of graph generated is solely dependent on the specific analysis required by the user. For this case we begin by recording the constants and provided parameters. The following maximization's will be utilized:

$$\max_{0\leq \mathrm{ALB}\leq 1} \mathrm{ALB} = 1$$

$$\max_{0\leq \theta\leq \pi/2} \cos\theta = 1$$

$$\max T_{\mathrm{eff}} = 315 \text{ K}$$

$$\max A_{\mathrm{cell}} = 1 \text{ m}$$

$$\min A_{\mathrm{p}} = 0 \text{ m}$$

These maximized parameters are displayed in the table below.

Thermal Parameters		
	Value	Unit
Beta Angle	0	degree
Solar Constant	1322	W/m^2
Albedo Factor	1	-
Stefan-Boltzmann Constant	5.67×10^{-8}	W/m^2K^4
Effective Earth Temperature	315	K

For the sake of simplicity and to maximize the absorptivity and emissivity values, we'll consider the panel to consist solely of cells. Additionally, we will assume the small satellite operates at zero efficiency with maximum draw, resulting an estimated upper limit on the internal heat value of 20 W. The following maximized values associated with a panel will be employed.

Solar Panel Parameters			
	Modeled Area (m^2)	Absorptivity	Emissivity
Solar Panel	0	0.150	0.050
Solar Cell	1	0.637	0.900
Effective	1	0.419	0.520

Based on maximizing the satellite's heat intake, the value of $Q_{in} = Q_{rad}$ is approximately 420 W, corresponding to an operational temperature of roughly 490 K. For context, typical operational temperatures for satellites in low Earth orbit range from 263 K to 333 K.

IV. RADIATOR MATERIAL CANDIDATE MODEL

A. Overview

With an accurate, steady state, thermal environment including reliable temperature outputs established, we add to the model's framework for the purpose of testing materials in the LEO environment. In this phase, we have begun identifying state-of-the-art radiator material options as we develop the model. For LEO applications, it's crucial to choose materials with excellent thermal conductivity, high emissivity, and resistance to atomic oxygen (AO). The fluctuation in solar activity affects AO density, which in turn can accelerate material erosion and deformation when directly exposed [6]. Furthermore, enhancing thermal emittance can involve altering surface morphology through texture introduction and applying coatings of varying thickness [7]. There are seven criteria in which the material's thermal conductivity can be maximized, these items are listed below.

i. Temperature: In metallic-like materials, thermal conductivity typically decreases with rising temperatures. This decrease occurs due to increased vibration among solid-state particles, which in turn leads to higher resistance.

ii. Density: Increased atomic density within a crystal lattice correlates with higher thermal conductivity. This is attributed to the enhanced efficiency of heat transfer facilitated by charge carriers such as phonons or electrons.

iii. Pressure: When a material experiences a significant increase in pressure, it's probable that its density will also increase. Additionally, if this pressure causes a phase transition, the resulting phase may exhibit higher thermal conductivity.

iv. Composition: The composition of atoms, molecules, or ions significantly influences a material's thermal conductivity. Materials containing free charge carriers, like metals, facilitate easy heat transfer.

v. Structure: The lattice structure is crucial in determining a material's thermal conductivity. Larger crystals excel at transferring energy because they have fewer grain boundaries, which enables charge carriers to move more freely.

vi. Porosity: When a material has more gaps or pockets unrelated to its crystal lattice, its thermal conductivity tends to decrease. This principle also applies to porosity, akin to the concept of grain boundaries.

vii. Impurities: When materials contain substantial impurities of any type, they undergo ionized impurity scattering. This phenomenon involves the scattering of charge carriers due to ionization within the lattice, which obstructs their path and results in decreased thermal conductivity.

Considering these characteristics and the demand for high-temperature applications, we chose to conduct experimental investigations on carbon structures. Specifically, we gather experimental data on carbon nanotubes (CNTs) as part of this model's framework. We anticipate

conducting additional tests on a range of materials in the future.

B. Material Modeling Process

In space, where a near-perfect vacuum prevails, heat transfer primarily occurs through radiation. However, employing a thermal conduction device can enhance heat transfer efficiency. This process can be accurately modeled by leveraging concepts from literature that pertain to thermal conductivity. Equation (18) demonstrates the net rate of heat transfer via radiation.

$$\frac{Q_{net}}{t} = \sigma \varepsilon A(T_2^4 - T_1^4) \tag{18}$$

In this context, σ represents the Stefan–Boltzmann constant, ε denotes the emissivity of the material, A stands for surface area, T_2 signifies the radiator's temperature, and T_1 represents the temperature of the surrounding thermal environment. Equation (19) illustrates the rate of heat transfer within a material through conduction.

$$\frac{Q}{t} = \frac{kA(T_2 - T_1)}{d} \tag{19}$$

Where A represents the surface area of the conductive material, d indicates its thickness, T_2 denotes the hot temperature, T_1 denotes the cold temperature, and k signifies the thermal conductivity of the radiator material, which is typically determined through experimentation. To ascertain a thermal conductivity value not found in literature, we first considered the most cost effective approach. The Wiedemann-Franz law postulates that the ratio of a metal's thermal conductivity to its electrical conductivity is directly proportional to temperature [4]. These seemingly disparate properties are interconnected through the presence of free electrons within the material. By treating the metal akin to a classical gas and comparing the resultant conductivities, we can derive the relationship.

$$\kappa = \frac{n\langle\nu\rangle\lambda k}{2} \tag{20}$$

$$\sigma = \frac{ne^2\lambda}{m\langle\nu\rangle} \tag{21}$$

Here, κ represents thermal conductivity, and σ stands for electrical conductivity. By utilizing the formula for mean particle velocity from kinetic theory, we derive Equation (22).

$$\langle\nu\rangle = \sqrt{\frac{8kT}{\pi m}} \tag{22}$$

This ratio can be related to temperature and demonstrates the Wiedemann-Franz law. This can be seen quantitatively in Equation (23).

$$\frac{\kappa}{\sigma} = \frac{4k^2T}{\pi e^2} = LT \tag{23}$$

Here L is a proportionality constant known as the Lorenz number.

$$L = \frac{\kappa}{\sigma T} = \frac{\pi^2 k^2}{3e^2} = 2.45 \times 10^{-}8\ W\Omega/K^2 \tag{24}$$

We aim to apply this theory to a nonmetallic semiconductor for its informational advantages. Specifically, this allows us to conduct experiments on electrical conductivity and simultaneously determine thermal conductivity.

C. Results

Two brass strips are adhered to a strip of CNT. Voltage measurements are taken as current passes through the material. A resistor is substituted to adjust electrical resistance. We test two CNT sheets with paper weights of 20 g/cm^2 and 60 g/cm^2. Both samples measure 30 mm in length, 5 mm in width, 250 μm in thickness, and have a cross-sectional area of $1.25 \times 10^{-}6$ m^2. Below are the tables and corresponding graphs for each test.

CNT 20 g/cm^2		
Resistance (Ω)	Current (μA)	Voltage (mV)
0	0	0
4.87	0	24.34
19.47	0	97.36
452.73	4.87	2263.64
890.85	9.74	4454.25
900.59	9.74	4502.93
1212.14	14.60	6060.70
1986.16	29.21	9930.79
2477.83	34.08	12389.15
2482.70	24.34	12413.49
3762.99	53.55	18814.96
4692.79	73.02	23463.93

CNT 60 g/cm^2		
Resistance (Ω)	Current (μA)	Voltage (mV)
0	0	0
4.87	0	24.34
19.47	0	97.36
447.86	63.28	2239.30
871.38	131.44	4356.89
881.11	126.57	4405.57
1173.20	175.25	5865.98
1883.93	287.21	9419.65
2312.32	355.37	11561.58
2312.32	350.50	11561.58
3402.76	516.01	17013.78
4162.17	627.98	20810.85

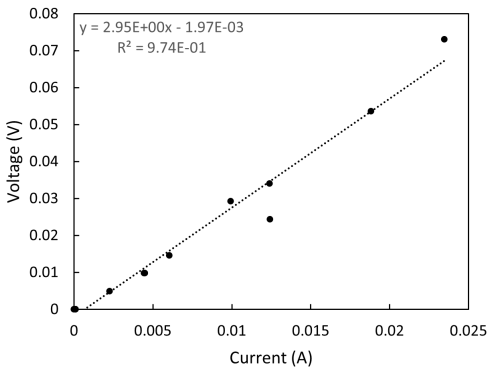

FIG. 4. Resistance slope for CNT 20g/cm^2

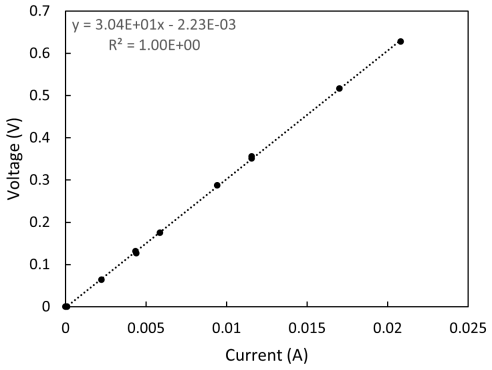

FIG. 5. Resistance slope for CNT 60g/cm^2

To calculate the the electrical conductivity we first find the resistivity using Equation (25).

$$\rho = \frac{RA}{L} \tag{25}$$

Here, R represents the resistance obtained from the slope of the voltage versus current graphs, A denotes the cross-sectional area, and L signifies the length of the material. Consequently, electrical conductivity is straightforwardly computed using Equation (26).

$$\sigma = \frac{1}{\rho} \tag{26}$$

The computed electrical conductivity values align with literature values for CNTs, typically ranging from approximately $10^2 - 10^3$ S/m. However, the thermal conductivity values do not match. Thermal conductance follows Fourier's law, where it is proportional to specific heat, sound velocity, and the mean free path of phonons. Heat transfer occurs via phonons, not electrons. Therefore, a quantum mechanical explanation involving elementary vibrational motion, where a lattice of atoms or molecules oscillates uniformly at a single frequency, is required to reconcile this model. More research on this topic is required. [5]. In the interim, we opt for the costlier approach involving the application of the Stefan-Boltzmann Law. This entails utilizing a Stefan-Boltzmann lamp housed within a vacuum chamber to replicate the thermal conditions encountered in space. Furthermore, the deployment of a thermal camera can be employed to directly record heat measurements.

V. CONCLUSION

The program's output results depicting the thermal environment meet the steady-state conditions typical of SmallSats in LEO. Specifically, we successfully replicated and demonstrated the thermal conditions applicable to ISISPACE's 3U SmallSat, as evidenced in Figure 3. Additionally, we have initiated testing theoretical values at elevated temperatures to assess their impact on the radiative process within these distinct environmental settings. Our efforts have led to the establishment of a mathematical model showcasing the efficacy of various radiative materials under these conditions. Leveraging the Wiedemann-Franz law, we explored a novel and cost effective experimental approach to derive thermal conductivity values, a method not currently addressed in existing literature but potentially forthcoming. Looking ahead, we anticipate identifying the most promising materials for each thermal environment, though refinement will be necessary before progressing to the experimental phase. The modeling process remains dynamic and subject to iterative changes. Upon completing the initial modeling phase, we aim to elevate the technology readiness level of multiple materials from a design-focused stage (TRL 3) to one involving component testing (TRL 4) [6]. Future investigations will concentrate on further refining the model, transitioning it into a time-dependent system to capture dynamic thermal behaviors accurately. Concurrently, ongoing efforts involve the exploration and evaluation of various structural design alternatives to optimize performance and efficiency.

ACKNOWLEDGMENTS

This research was supported by the University of Central Florida under the direction and supervision of Ali P. Gordon, Ph.D., Jeffrey L. Kauffman, Ph.D., Kawai Kwok, Ph.D., Maxwell Booth, and Bojan Bijelic, with further support from the National Science Foundation and the Department of Defense.

[1] I. Foster, *Small Satellite Thermal Modeling Guide*, Tech. Rep. (Kirtland AFB, NM, 2022).

[2] A. H. Carter, *Classical and Statistical Thermodynamics* (Prentice Hall, Upper Saddle River NJ, 2001).

[3] 7.0 thermal control (2021).

[4] W. Jones, *Theoretical Solid State Physics* (Dover Publications, New York, 2001).

[5] S. H. Simon, *The Oxford Solid State Basics* (CPI Group, Croydon EN, 2013).

[6] I. Tzinis, Technolgy readiness level (2021).

[7] P. Nogueira, *Micro-Satellite Electrical Power Subsystem Design and Test*, Ph.D. thesis (2017).

[8] K. D. Stout, *Design optimization of thermal paths in Spacecraft Systems*, Ph.D. thesis, Cambridge MA (2013).

[9] W. Mahmoud, D. Elfiky, and S. Robaa, Effect of atomic oxygen on leo cubesat, International Journal of Aeronautical and Space Sciences **22**, 1 (2021).

[10] S. K. Rutledge, B. A. Banks, M. J. Mirtich, R. Lebed, J. Brady, D. Hotes, and M. Kussmaul, *High Temperature Radiator Materials for Applications in the Low Earth Orbital Environment*, Tech. Rep. (Cleveland OH, 1987).

[11] I. Martínez, Spacecraft thermal control (1995-2023).